ABSTRACT

Title of Thesis:	ATOMIC LAYER DEPOSITION OF NICKEL THIN FILMS FOR SPACECRAFT OPTICAL APPLICATIONS
	Ching-En Ku, Master of Science
Thesis Directed By:	Professor Raymond A. Adomaitis, Department of Chemical and Biomolecular Engineering and Institute for Systems Research

Two approaches for Ni Atomic Layer Deposition on glass substrates have been studied for spacecraft optical applications. The first strategy is to first deposit a NiO thin film and then reduce the metal oxide film using noble gas under high temperature. $NiCp_2$ and O_3 as the precursors were chosen due to the low-temperature required for deposition and high growth rate. An alternative pathway was to deposit a Ru metallic film as the adsorption layer, using $Ru(DMBD)(CO)_3$ and H_2O, then deposit the Ni metallic film on the Ru film using $Ni(DAD)_2$ and tert-butylamine. The reaction mechanisms for both processes were developed. The ideal theoretical growth rates of

these ALD processes were calculated as 2.40 Å/cycle for NiO, 2.19 Å/cycle for Ru and 2.04 Å/cycle for Ni metallic film.

ATOMIC LAYER DEPOSITION OF NICKEL THIN FILM FOR USE IN SPACE OPTIC APPLICATIONS

by

Ching-En Ku

Thesis submitted to the Faculty of the Graduate School of the
University of Maryland, College Park, in partial fulfillment
of the requirements for the degree of
Master of Science
2020

Advisory Committee:
Professor Raymond A. Adomaitis
Professor Chen Zhang
Professor Dongxia Liu

© Copyright by
Ching-En Ku
2020

Table of Contents

Table of Contents ii

List of Tables iii

List of Figures iv

List of Abbreviation v

Chapter 1: Introduction 1

1. History 1
2. Principles of ALD 2

Chapter 2: Atomic Layer Deposition of Nickel oxide for use in X-ray optics 5

1. Introduction 5
2. Structure properties and theoretical growth rate 10

Chapter 3: Atomic Layer Deposition of Nickel metal thin films on ruthenium 14

1. Introduction 14
2. Reaction mechanism 17
3. Structure properties and theoretical growth rate 19

Chapter 4: Conclusions and Future Works 23

1. Conclusions 23
2. Future works 24

BiBliography 25

List of Tables

2.1 List of NiO ALD studies and the growth rate per cycle using $NiCp_2$ and O_3. .13

3.1 The experimental growth rate of Ni metallic thin films using $Ni(dad)_2$ and tert-butylamine. ………………………………………………………………...21

List of Figures

1.1 A general process of ALD. (a) Functionalized substrate surface. (b) Precursor A is pulsed and reacts with the surface. (c) Inert carrier gas purging with excess precursor and by-products of the reaction. (d) Precursor B is pulsed and reacts with the surface. (e) Inert carrier gas purging with excess precursor and by-products of the reaction. (f) Repeat steps (b) to (e) to achieve the desired thin film thickness. 4

2.1 The illustration of X-ray optical system using a spherical slumped microchannel plate. 6

2.2 The structure diagram of nickelocene. 8

2.3 Reaction mechanism for the nucleation phase of the proposed ALD growth. 10

2.4 Reaction mechanism for the growing phase of the proposed ALD growth. 10

2.5 The experimental data of the growth rate of NiO ALD. 13

3.1 Structure diagram of Ru(DMBD)$(CO)_3$. 16

3.2 Structure diagram of $Ni(DAD)_2$. 16

3.3 Structure diagram of tert-butylamine. 16

3.4 Reaction mechanism for the Ni ALD process. 19

3.5 Hexagonal close packed crystal structure of Ru. 20

List of abbreviation

ALD	Atomic Layer Deposition
ALE	Atomic Layer Epitaxy
$Co(DAD)_2$	Bis(1,4-di-tert-butyl-1,3-diazadienyl)Cobalt
CNT	Carbon Nanotube
CVD	Chemical Vapor Deposition
DFT	Density Function Theory
fcc	Face Centered Cubic
gpc	Growth Per Cycle
hcp	Hexagonal Close Packed
$Ni(acac)_2$	Nickel(II)acetylacetonate
$Ni(apo)_2$	Nickel(2, amio-pent-2-en-4-onato)
$Ni(Cp)_2$	Nickelocene
$Ni(DAD)_2$	Bis(1,4-di-tert-butyl-1,3-diazadienyl)nickel
$Ni(dmg)_2$	Nickel Dimethylglyoxime
NiO	Nickel Oxide
$Ru(Cp)_2$	Ruthenocene
$Ru(DMBD)(CO)_3$	η^4-2,3-dimethyl Butadiene Ruthenium Tricarbonyl
$Ru(EtCp)_2$	Bis(ethylcyclopentadienyl)ruthenium(II)
$Ru(thd)_3$	Tris(2,2,6,6-tetramethyl-3,5-heptanedionato)ruthenium(III)
$tBuNH_2$	tert-Butylamine
XPS	X-Ray Photoelectron Spectroscopy
XRD	X-Ray Diffraction

Chapter 1: Introduction

Atomic Layer Deposition (ALD) is a gas-phase thin film deposition technique in which the gas precursors of ALD are fed separately to the reactor to prevent gas phase reactions, that has been widely investigated in various fields including semiconductor applications, astronomical optics, energy and environmental devices and biological applications.[1–7] ALD has demonstrated several advantages over other thin film deposition techniques. ALD can produce a constant deposited film thickness for every cycle, also known as growth rate per cycle, due to its self-limiting behavior. Moreover, the availability for gas precursors to deposit on any substrate with active surface sites results in the broadly applicability of ALD. The film thickness can be adjusted by changing the total number of ALD cycles, with the precise nanoscale control of film deposition, highly conformal thin films with desired thickness and properties can be obtained.[5,8–10]

1. History

The concept of ALD was introduced by two different researchers, T. Suntola reported a technique known as “atomic layer epitaxy” in 1977 for electroluminescent flat panel displays, and the other origin is attributed to S. Koltsov under the name

"molecular layering" in 1965.[5] The ALD technique was first put into practice in 1983 as an electroluminescent display at Helsinki airport and was first applied in commercial use as an ALE reactor called F-120 in 1988.[3] The transition from using the word "ALE" to a more general name "ALD" occurred in the late 1990s because most of the film is grown using self-limiting sequential reactions that were not epitaxial to the underlying substrates. In the early years, due to the lack of requirements of precise control for thin film deposition at atomic scale, researchers proceeded slowly in developing new ALD techniques. Things started to change in the late 1990s with the continuing downsizing of electronic device, requiring a new deposition method with the ability to coat high quality, conformal accurate film for precise control at atomic level. ALD is one of the suitable techniques to achieve this requirement. Nowadays, ALD has been developed to be applied in many different fields of studies such as semiconductor industries, biomedical studies and environmental applications.[1–7]

2. Principles of ALD

ALD is a deposition technique in which the film is grown by exposing the substrate to gas precursors. It is a branch of the chemical vapor deposition (CVD) technique. The main difference between ALD and the traditional CVD technique is that the gas precursors in the ALD process are fed separately in time so that the gas-phase

precursors are never present simultaneously in the reactor to prevent any uncontrolled gas-phase reactions. This process leads to the characteristic that the gas precursors only react with the surface and each half-reaction terminates when all the reaction active sites on the surface are occupied. The self-limiting behavior is influenced by the complete consumption of active sites and the steric hindrance caused by large ligands of the adsorbed precursor, which will prevent any additional precursor to be adsorbed to the substrate. By designing a good ALD precursor system, the coated film after a precursor pulse provides an activated surface for the following precursor for reaction and adsorption. A film with the desired thickness can then be obtained by repeating the ALD cycles.[11]

ALD process can be shown as Figure 1.1. The process includes sequential pulses of gaseous precursors with the substrate. First, the first precursor will be fed to the reactor. When the gas precursor contacts the reaction surface with active sites, the precursor is adsorbed onto the substrate until the precursor is chemically bonded. Note that the transportation of the gaseous precursor is supported through the vapor pressure itself, or an inert gas such as argon or nitrogen will be induced to increase the rate of transport from the source to the reactor. After the first precursor pulse, the inert gas will be pulsed into the reaction chamber to remove excess precursors and the byproducts of the reaction between the precursor and the surface. With the inert gas purging, we can

ensure that the reaction will only occur between the gas precursor and the film surface. Then the other precursor will be fed to the chamber, for an effective precursor system, the surface deposited by the first precursor most provide reaction active sites for the second precursor to be adsorb and react. The process will be repeated until the desired thickness is achieved.[12]

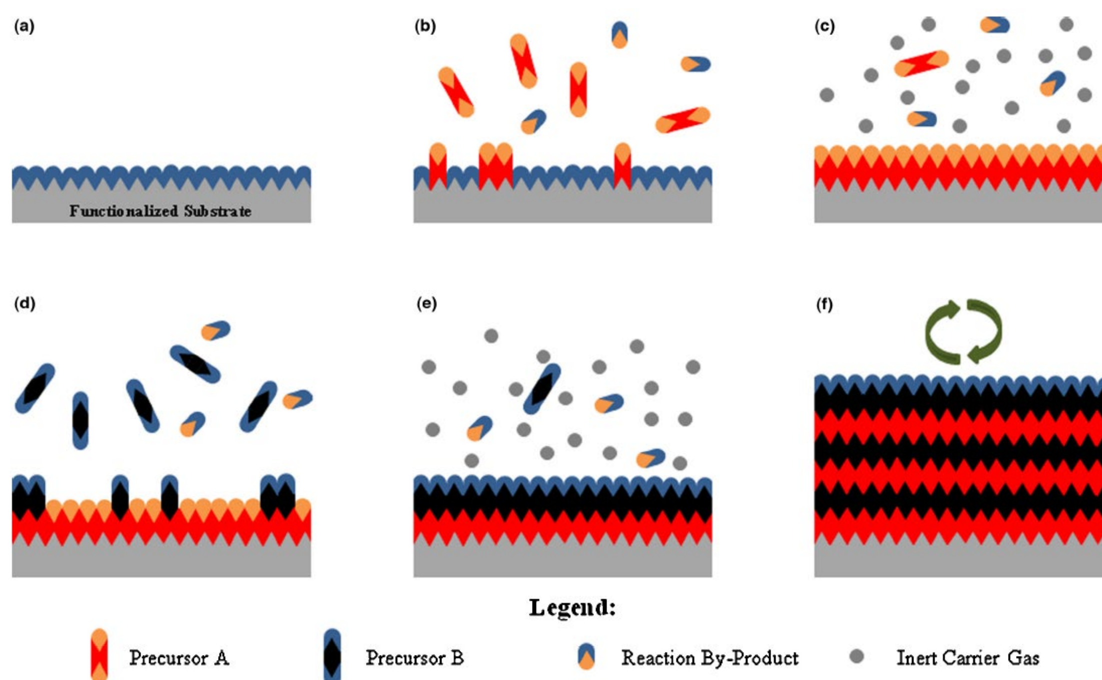

Figure 1.1. A general process of ALD. (a) Functionalized substrate surface. (b) Precursor A is pulsed and reacts with the surface. (c) Inert carrier gas purging with excess precursor and by-products of the reaction. (d) Precursor B is pulsed and reacts with the surface. (e) Inert carrier gas purging with excess precursor and by-products of the reaction. (f) Repeat steps (b) to (e) to achieve the desired thin film thickness. [Reprinted from ref [12]]

Chapter 2: Atomic Layer Deposition of Nickel oxide for use in X-ray optics

1. Introduction

Observational astronomy of X-ray emission from the astronomical objects is known as X-ray astronomy. When the emitted X-ray entered the atmosphere of earth, most of the emission will be absorbed by our atmosphere. To avoid this issue, X-ray detectors are usually set at high altitudes such as sounding rockets and satellites so that the telescope avoids the influence of the atmosphere and receives X-ray radiation directly.

The lobster-ISS X-ray imaging detector is an X-ray optical system described by JK.Black.[13] The lobster-ISS is an all-sky monitor of X-rays which can maps the entire sky approximately every 90 minutes with excellent sensitivity. It is planned to be attached to the International Space Station. The X-ray detector is constructed by using a wide-field X-ray focusing element which is shown in Figure 2.1, which includes a spherical focal surface and a spherically slumped microchannel plate. To redirect the source X-ray onto the spherical focal surface, the incoming X-ray needs to be reflected from the inner surface of microchannel to focus and form the image of the X-ray source. On the top of the channel surface, Ni metallic film is deposited to increase the X-ray reflectivity.

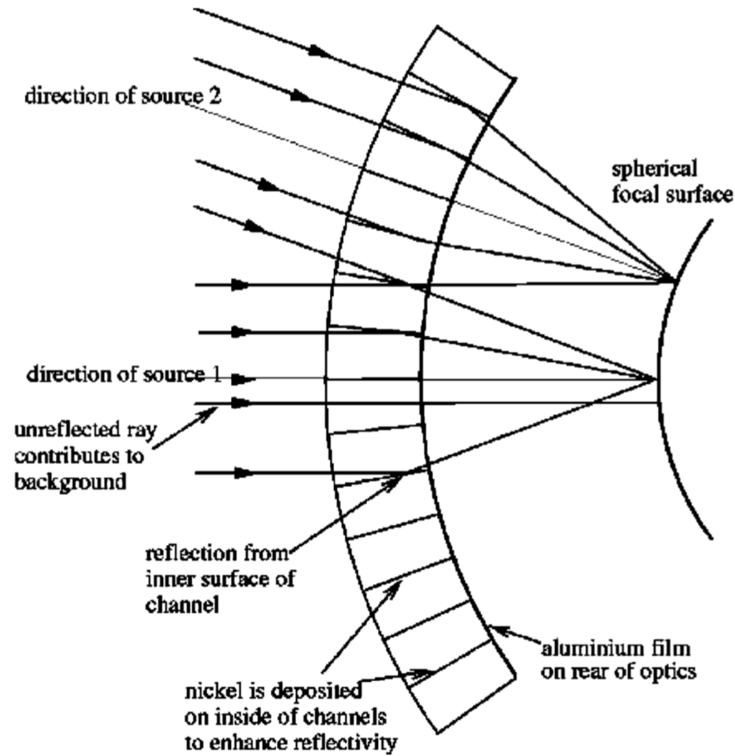

Figure 2.1: The illustration of X-ray optical system using a spherical slumped microchannel plate. (Reprinted from ref [13])

Recently, scientists are working to develop an ALD process to deposit the Ni thin film on the glass optical element. Since ALD can provide a highly conformal coating of metallic thin film with desired thickness, the use of ALD process gives the potentials for a new generations of X-ray optics applications. Therefore, investigating reaction mechanisms for Ni ALD process is significant.

The main challenge of metallic Ni thin films ALD is that directly depositing pure Ni films on substrates is difficult. High temperature processes are usually needed due to the Ni precursors resistance to reduce to its metallic state. In addition, surface

energies of metallic thin films and glass substrate differ greatly, which leads to a relatively long nucleation period and large grain size. To avoid these issues, there are several strategies that can be taken for Ni ALD deposition. One of the approaches is to first deposit NiO thin film and then process a reduction reaction using noble gas such as hydrogen and argon. The advantages of this strategy are that NiO deposition can be proceed at a relatively low temperature and a short nucleation period can be obtained.

Considerable studies have been done to understand the NiO ALD reaction. Nickel(II)acetylacetonate, also known as $Ni(acac)_2$ is a widely used nickel precursor. It is first introduced by Utriainen et al.[14] They used $Ni(acac)_2$ and H_2O as the precursors for NiO growth and then converted it to metallic Ni film by a reduction step by using hydrogen. $Ni(dmg)_2$, also known as nickel dimethylglyoxime and $Ni(apo)_2$, also known as nickel(2, amio-pent-2-en-4-onato), were also used to react with different oxygen precursors such as O_3 and H_2O.[15] However, these precursors have been found to have poor gas phase stability. For example, $Ni(acac)_2$ has been indicated to have a strong tendency to form trimers in gas phase, which would complicate the precursor delivery system design.[15] Lu et al. report a good precursor system which provides promising high-quality metal oxide films using nickelocene as shown in Figure 2.2., or $Ni(Cp)_2$ and ozone.[15] The structure diagram of $Ni(Cp)_2$ is shown in Figure 2.2, the oxidation state of Ni is +2. Bachmann et al. investigated the stoichiometry and the chemical

composition of Ni and NiO thin films.[16] In their study, NiO film was grown on silicon(100) wafers by a nickelocene ALD process, and then the argon appealing process under high temperature (700℃) was proceeded. The morphology of the film was changed and the film was converted to Ni metallic film. Wen et al. studied the reaction kinetics and selective growth of metal oxide ALD process on Pt nanoparticles using $NiCp_2$ and O_3.[17] They proposed an adsorption-dissociation reaction mechanism and predicted the selectivity of growth rate on different facets of Pt substrate. Nickelocene can also be used as a nickel precursor for NiO growth on carbon nanotubes.[18,19] The NiO thin film deposited on carbon nanotubes is shown to be conformal with a relatively high growth rate comparing with other precursor systems, resulting in films with high electrochemical performance and excellent conductivity.

This project aims to study the reaction mechanism and the film properties of NiO atomic layer deposition growth on silicon oxide substrates. The motivation of this is to give us a better understanding of NiO ALD processes and ultimately apply the optimized process to enhance the reflectivity of X-ray optics.

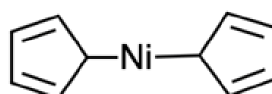

Figure 2.2. The structure diagram of nickelocene.

2. Reaction mechanism

In order to understand the reaction mechanism for nickel oxide growth on a silicon oxide substrate, we can gain insight from comparing this precursor system to similar ALD systems of other oxides and substrates since there is little information available. Surface reaction mechanism of NiO deposition has been studied on different substrates using the same precursor system.[17] Wen et al. has reported that it is most likely for the $Ni(Cp)_2$ half-cycle that the reaction consists of an adsorption step for the precursor and a dissociation step for Cp ligand. The SiO_2 surface is treated hydroxylated, the hydroxyl groups on the silicon oxide surface can serve as the active sites for reacting with Ni precursors. Consequently, this half pulse cycle can be considered as

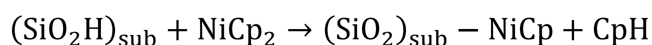

$$(SiO_2H)_{sub} + NiCp_2 \rightarrow (SiO_2)_{sub} - NiCp + CpH$$

sub subscript refers to the growing substrate. $(SiO_2H)_{sub}$ represents the hydroxylated SiO_2 surface. Note that in this half-cycle reaction, there is a Cp ligand dissociated from the nickel precursor after the precursor is adsorbed on the substrate.

During the O_3 half cycle, the Cp ligand remaining on the growth surface should be oxidized by ozone and form NiO. It was suggested by Wen et al. that the oxidation process can produce CO_2 and H_2O.[17] Therefore, the ozone pulse reaction can be shown as

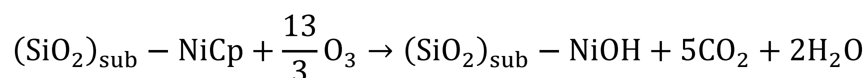

$$(SiO_2)_{sub} - NiCp + \frac{13}{3}O_3 \rightarrow (SiO_2)_{sub} - NiOH + 5CO_2 + 2H_2O$$

Thus the overall reaction is then

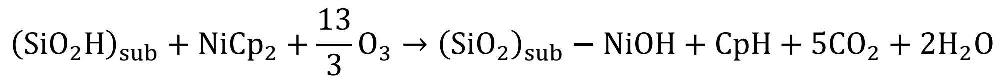

$$(SiO_2H)_{sub} + NiCp_2 + \frac{13}{3}O_3 \rightarrow (SiO_2)_{sub} - NiOH + CpH + 5CO_2 + 2H_2O$$

A complete diagram for reaction mechanisms for our precursor system is illustrated in Figure 2.3 and Figure 2.4, note that the coordination number of Ni^{2+} in NiO ALD films is 6.

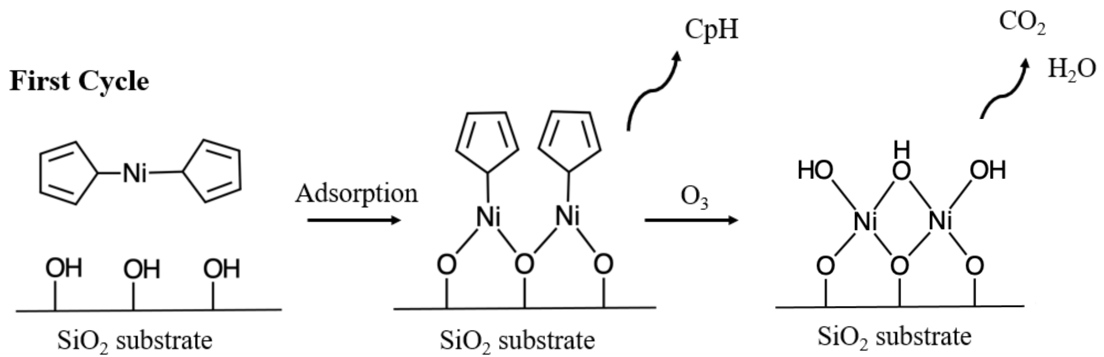

Figure 2.3: Reaction mechanism for the nucleation phase of the proposed ALD growth.

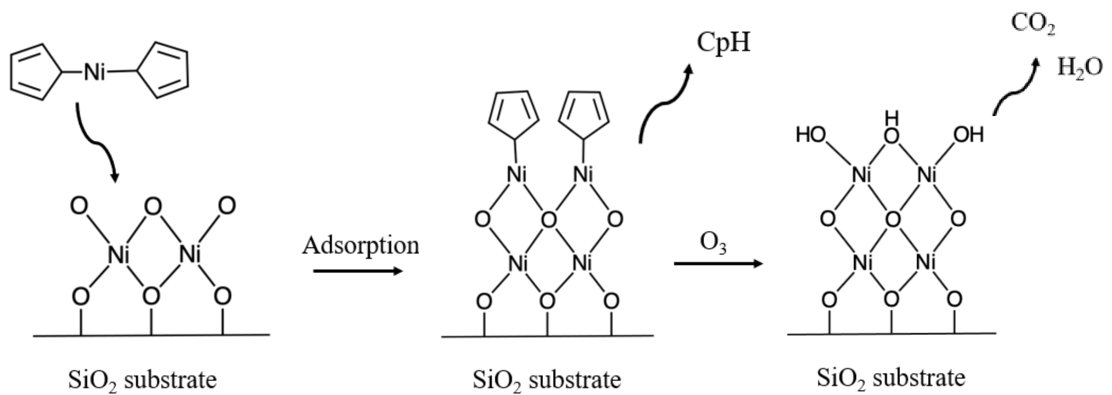

Figure 2.4: Reaction mechanism for the growing phase of the proposed ALD growth.

3. Structure properties and theoretical growth rate

To understand the structure of NiO thin film, it is important to review the characterization of nickelocene precursor system deposited films studied by previous

researchers. In the ALD process of Bachmann et al., NiO thin films were prepared by nickelocene and ozone at 230℃ on Si(100) substrates, with a measured growth per cycle of 0.92 Å/cycle.[16] The film structure information was studied by X-ray diffraction (XRD), an analytical technique which is often used to determine the crystalline structure of materials. In their study, three peaks are observed, which corresponds to the (111) (200) and (220) lattice planes of nickel oxide. This result leads to the conclusion that the crystal structure of NiO is face-centered cubic (fcc). Similar XRD patterns can also be obtained in other studies using the same precursor system. Lu et al. carried out their experiments within the temperature range of 150-300℃ on a Si(100) substrate, and Yu et al. operated their deposition under 150℃ on carbon nanotubes (CNT).[15,18] In all of these characterization studies results obtained by XRD showed similar peaks, which indicates that the molecular structure of NiO deposited film is fcc in nature under the range of deposition temperatures and substrates represented in those studies. Additionally, Lu et al. have reported that there is likely an increasing trend of crystallinity as deposition temperature increases.

Having established the fcc structures for NiO films, the theoretical growth rate per cycle can be calculated in the following manner:

Definition of cubic crystal's density:

$$\rho = \frac{4 \times M_{Ni} + 4 \times M_{O}}{a^3 \times N_A}$$

where ρ represents the density of the compound (g/cm^3), a represents the cubic length (Å), N_A represents the Avogadro's number (mol^{-1}) and M represents the molar mass of the compound (g/mol). Cubic length can then be calculated as

$$a = \sqrt[3]{\frac{4 \times M_{Ni} + 4 \times M_O}{\rho \times N_A}} = \sqrt[3]{\frac{4 \times 58.69 + 4 \times 16.0}{6.68 \times 6.023 \times 10^{23}}} = 4.156 \times 10^{-8}\mathrm{cm} = 4.156\ \text{Å}$$

We are calculating the theoretical growth per cycle under ideal condition, which the active sites on the surface are completely occupied for every precursor pulse. Due to the structure of fcc, the NiO film is growing along the perpendicular direction of (111) lattice plane. Therefore, the theoretical growth rate per cycle can be calculated as

$$\mathrm{gpc} = \frac{a}{\sqrt{3}} = 2.40\ \text{Å}$$

Table 2.1. lists NiO ALD experimental studies using the $Ni(Cp)_2/O_3$ precursor system and the growth rate per cycle that has been obtained in each. The calculated theoretical gpc is consistent with the experiment data deposited at ~250°C on Si(100) substrates. There are plenty of reasons that cause the difference in gpc. First, as mentioned in Chapter 1, it is most likely due to the steric hindrance caused by large segments of adsorbed precursor, which will prevent any additional precursor to be adsorbed to the substrate. Insufficient purge time between precursor pulses may also be a reason, the previous precursor or any byproduct may remain in the reactor, which leads to the occurrence of any gas-phase reaction and uncontrollable growth. Another probable reason is the depletion of precursor before the active sites on the substrates

have been completely reacted, which results in lower growth rate.

Table 2.1: List of NiO ALD studies and the growth per cycle using $NiCp_2$ and O_3.

Ref.	Substrate	Temperature	Growth per cycle
Bachmann et al.[16]	Si(100) wafer	230°C	0.92 Å
Lu et al.[15]	Si(100) wafer	150°C	3.2 Å
Lu et al.[15]	Si(100) wafer	200°C	2.5 Å
Lu et al.[15]	Si(100) wafer	250°C	1.2 Å
Lu et al.[15]	Si(100) wafer	300°C	0.8 Å

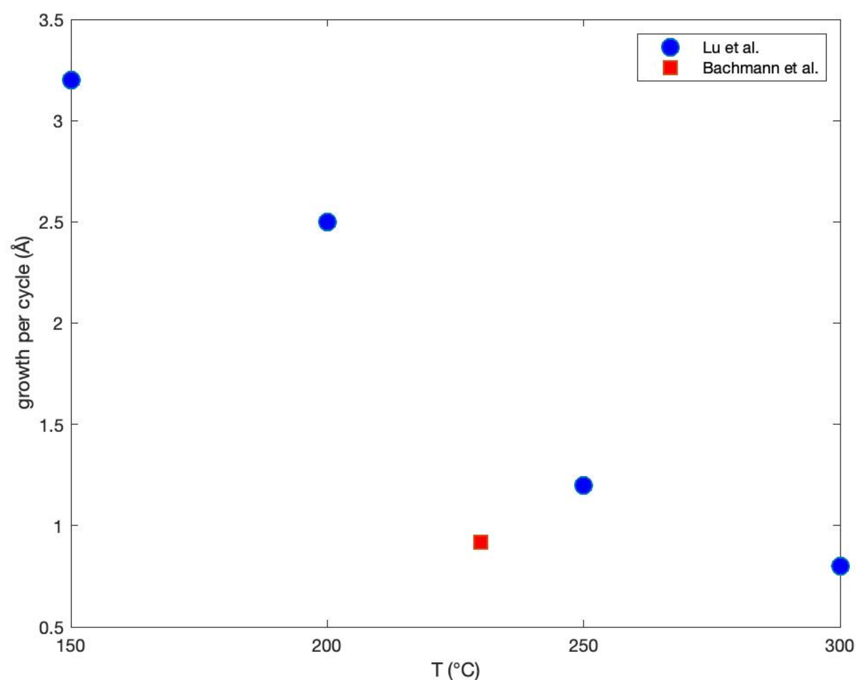

Figure 2.5: The experimental data of the growth rate of NiO ALD.

Chapter 3: Atomic Layer Deposition of Nickel metal thin films on ruthenium

1. Introduction

In the previous chapter, it was discussed that metallic Ni itself does not grow well on a glass substrate. While one of approach is to first grow a NiO thin film on the glass substrate and then reduce the NiO to Ni metallic film, it was found the reduction process would result in forming Ni clusters and losing the film continuity. An alternate approach is to add an adhesion layer such as platinum or ruthenium first on the glass substrate, then deposit the Ni metallic thin film on the adhesion layer. By following this strategy, it is possible to deposit a Ni thin film on the glass substrate. The thickness of Ru thin film should only be a few layers of deposition, while the thickness of Ni in our application is required as 25 nm. So the enhancement of X-ray reflection should not be affected.

In the past years, several ruthenium precursors have been reported to deposit metallic Ru films including metallocene, such as $Ru(Cp)_2$ and $Ru(EtCp)_2$ and β-diketonate precursors, such as $Ru(thd)_3$.[20,21] The films obtained from these precursors with an oxidation state of Ru center +3 or +2 were found to have promising properties, for example, low resistivity and low impurity concentrations. However, Hong et al.

have reported that the Ru ALD process with these precursors had a long incubation period and low film growth rate at the initial stages of film deposition.[22] The delayed nucleation leads to the rough morphology of deposited Ru films, which is not suitable for X-ray optical applications that require high conformality and low roughness. To solve this issue, zero-valent Ru precursors have been found to significantly enhance nucleation and provides excellent conformality with a smooth film surface. η^4-2,3-dimethyl butadiene ruthenium tricarbonyl, also known as Ru(DMBD)$(CO)_3$, has been introduced as such a zero-valent Ru precursor.[23] Gao et al. reported a Ru ALD process using Ru(DMBD)$(CO)_3$ and water with a low-temperature ALD window and high deposition rate (0.1 nm/cycle). They obtained a conformal, smooth Ru thin film with low electrical resistivity on SiO_2 substrate. The deposition mechanism on Si substrates has been studied using mass spectrometry and density functional theory calculations. Another precursor system, $C_{16}H_{22}Ru$ and O_2, is reported Eom et al. Yeo et al. studied the ALD reaction using $C_{14}H_{18}Ru$ and O_2.[24,25] Both the ALD process showed similar growth rates, 0.1 nm/cycle for using $C_{14}H_{18}Ru$ and 0.086 nm/cycle for using $C_{16}H_{22}Ru$, and short incubation periods. The key difference between these precursor systems is the optimized deposition temperature: the ALD temperature window of using Ru(DMBD)$(CO)_3$ is obtained at 160°C~210°C, while both $C_{16}H_{22}Ru$ and $C_{14}H_{18}Ru$ grow better when temperature is above 220°C. Ru(DMBD)$(CO)_3$ and H_2O are selected

as the precursor system is our study due to its low ALD temperature window.

Other precursor systems have been studied for growing Ni metallic films. $Ni(iPrNCMeNiPr)_2$ was used with H_2 as ALD precursors, $Ni((Me)(iPr)COCNtBu)_2$ and $BH_3(NHMe_2)$ have also been used as a precursor system for Ni thin film growing on SiO_2, but the growth rate was also found to be low (0.09 Å/cycle).[26,27] To overcome this issue, Kerrigan et al. introduced a prospective precursor system, bis(1,4-di-tert-butyl-1,3-diazadienyl)nickel, also known as $Ni(dad)_2$ and tert-butylamine, which provides a smooth film with a high growth rate under low deposition temperature.[28]

The aim of this chapter is to link the Ru and Ni deposition processes together as a new and novel method for generating a conformal nickel coating.

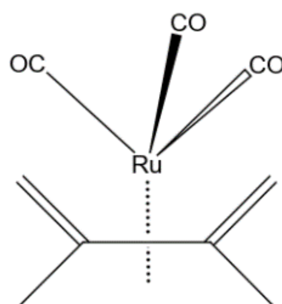

Figure 3.1: Structure diagram of $Ru(DMBD)(CO)_3$.

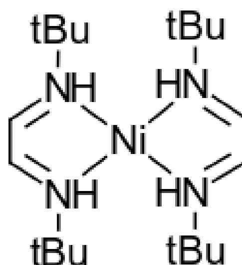

Figure 3.2: Structure diagram of $Ni(DAD)_2$.

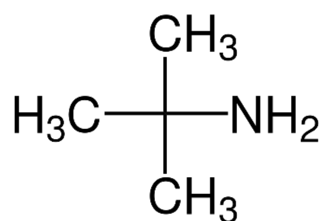

Figure 3.3: Structure diagram of tert-butylamine.

2. Reaction mechanism

The reaction mechanism of Ru ALD using Ru(DMBD)$(CO)_3$ and H_2O has been well studied by Gao et al.[23] They studied the mechanism of Ru deposition on a Si substrate by combining mass spectrometry and density functional theory (DFT) calculations. From mass spectrometry analysis, they indicated that the DMBD ligand dissociates when the precursor is adsorbed to the hydroxylated surface during the Ru(DMBD)$(CO)_3$ half cycle, and CO_2 is produced during both DMBD cycle and H_2O cycle. The conversion from carbonate ligand to CO_2 is a form of water-gas-shift reaction (WGSR). The CO_2 and H_2 are formed by either the CO ligand interacting with surface hydroxyl groups during Ru(DMBD)$(CO)_3$ half cycle, or the exposed CO groups on the adlayers interacting with H_2O during H_2O half cycle. A competitive process was also reported between DMBD ligand's and carbonyl group's interactions with hydroxyl groups on the surface. In our study, we are depositing Ru thin film on the glass substrate, thus from the study done by Gao et al., the reaction mechanism of Ru(DMBD)$(CO)_3$ half cycle is expected as follow:

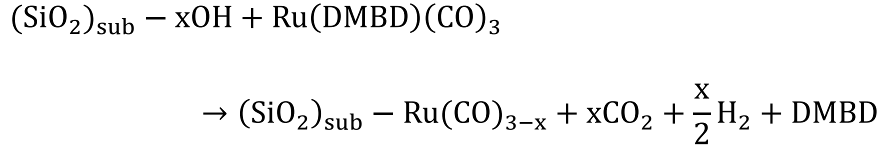

$$(SiO_2)_{sub} - xOH + Ru(DMBD)(CO)_3 \rightarrow (SiO_2)_{sub} - Ru(CO)_{3-x} + xCO_2 + \frac{x}{2}H_2 + DMBD$$

The mechanism for the H_2O half cycle is expected as follow:

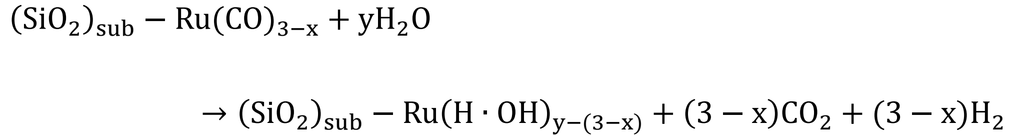

$$(SiO_2)_{sub} - Ru(CO)_{3-x} + yH_2O \rightarrow (SiO_2)_{sub} - Ru(H \cdot OH)_{y-(3-x)} + (3-x)CO_2 + (3-x)H_2$$

Where the $(SiO_2)_{sub} - Ru(H \cdot OH)_{y-(3-x)}$ indicates that the H_2O is adsorbed on the surface as a combination of H and OH groups.

For the Ni metallic thin film ALD using $Ni(dad)_2$ and tert-butylamine, while there is little information regarding the reaction mechanisms, we can gain insight from similar ALD systems of related metal precursors. A cobalt ALD process using $Co(dad)_2$ has been previously studied by Wolf et al.[29] XPS have been used to study the ALD using $Co(dad)_2$ and HCOOH. In this study, film surface composition was observed to increase with respect do carbon and decrease with respect to cobalt during HCOOH pulse, while an opposite trend was observed during the $Co(dad)_2$ half cycle. Similar patterns also occurred when tert-butylamine was used as a precursor. This result indicates the occurrence of ligand exchange. Therefore, for the $Ni(dad)_2$ half cycle in our study, the most likely mechanism of the nucleation phase is proposed as

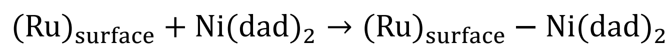

$$(Ru)_{surface} + Ni(dad)_2 \rightarrow (Ru)_{surface} - Ni(dad)_2$$

For the tert-butylamine half cycle, the reaction is then

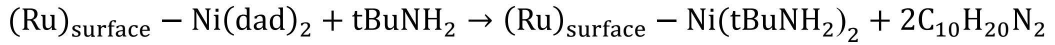

$$(\mathrm{Ru})_{\mathrm{surface}} - \mathrm{Ni(dad)_2} + \mathrm{tBuNH_2} \rightarrow (\mathrm{Ru})_{\mathrm{surface}} - \mathrm{Ni(tBuNH_2)_2} + 2\mathrm{C_{10}H_{20}N_2}$$

In the first half-reaction, the $Ni(dad)_2$ is simply adsorbed onto the Ru substrate. In the second half-cycle, a ligand exchange between tert-butylamine and dad ligand occurred. Therefore, the mechanism of $Ni(dad)_2$ half-cycle during growth phase can be shown as

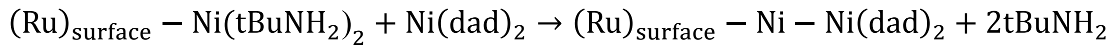

$$(\mathrm{Ru})_{\mathrm{surface}} - \mathrm{Ni(tBuNH_2)_2} + \mathrm{Ni(dad)_2} \rightarrow (\mathrm{Ru})_{\mathrm{surface}} - \mathrm{Ni} - \mathrm{Ni(dad)_2} + 2\mathrm{tBuNH_2}$$

The tert-butylamine half-cycle during the growth phase is then

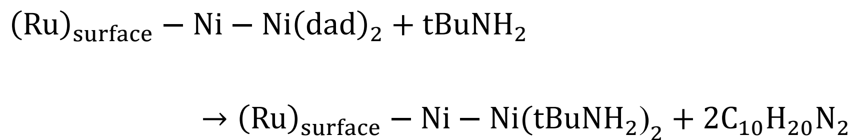

$$(\mathrm{Ru})_{\mathrm{surface}} - \mathrm{Ni} - \mathrm{Ni(dad)_2} + \mathrm{tBuNH_2} \rightarrow (\mathrm{Ru})_{\mathrm{surface}} - \mathrm{Ni} - \mathrm{Ni(tBuNH_2)_2} + 2\mathrm{C_{10}H_{20}N_2}$$

The schematic diagram can be illustrated in Figure 3.1

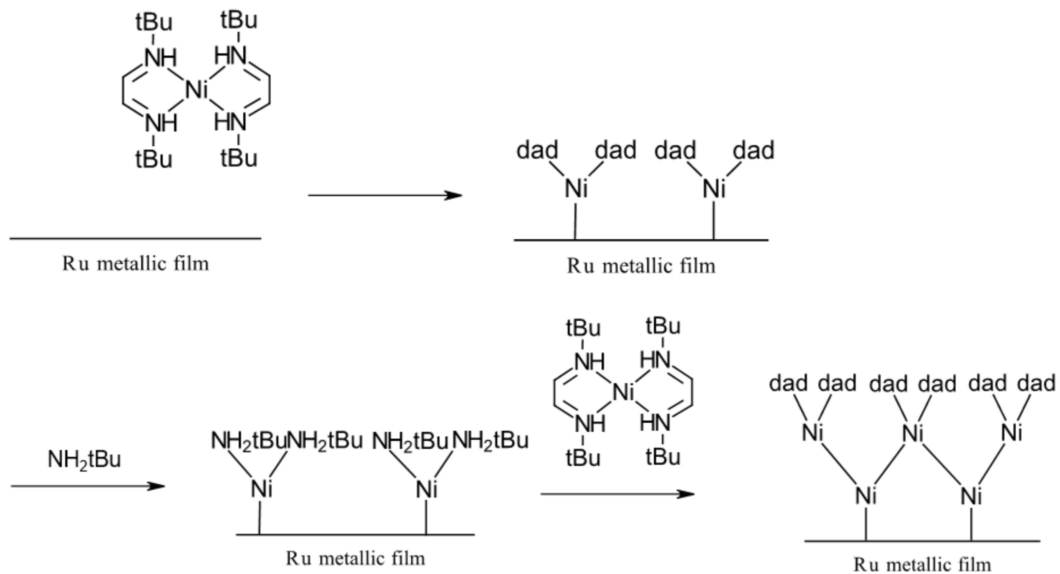

Figure 3.4: Reaction mechanism for the Ni ALD process.

3. Structure properties and theoretical growth rate

To investigate the crystal structure of Ru ALD thin films, XRD patterns have been

studied by hong et al. and Gao et al. where similar patterns were observed in both studies.[22,23] Several peaks were observed including the peaks corresponding to the (100), (002) and (101) lattice planes of Ru, which leads to the conclusion that the crystal structure of Ru is hexagonal close packed (hcp). The structure diagram is shown in Figure 3.2. We assumed that in ideal condition, the theoretical growth per cycle can be calculated as:

$$\overline{RQ} = \frac{2}{3}\cos\angle QRS\,\overline{PR} = \frac{2}{3}\cos 30°\,2r = \frac{2}{3}\sqrt{3}r$$

$$\overline{PQ} = \sqrt{\overline{PR}^2 - \overline{RQ}^2} = 2r\sqrt{\frac{2}{3}}$$

$$c = 2\overline{PQ} = 4r\sqrt{\frac{2}{3}}$$

$$\mathrm{r} = 1.34\text{Å}$$

Where r represents the radius of the ruthenium atom, so the length of Ru crystal structure is 4.376Å. From the hcp structure as shown in Figure 3.4, each hcp structure contains 2 layers of Ru films. Therefore, the growth rate of Ru can then be calculated as half of the crystal length as 2.188Å. By comparing the theoretical growth rate of Ru with the experimental data obtained by Gao et al. (1.0 Å), we can found that the experiment data is far smaller than the calculated growth rate.[23] As mentioned in the previous chapter, steric hindrance, precursor depletion and insufficient pulsing time may cause the different between experimental data and calculated growth rate.

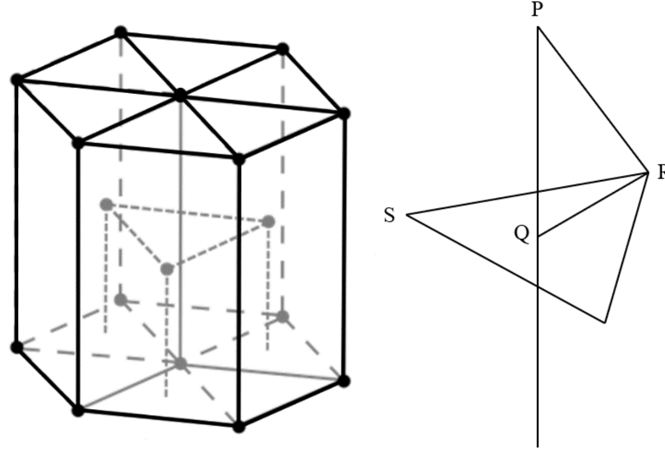

Figure 3.4: Hexagonal close packed crystal structure of Ru.

For the Ni ALD process, characterization of Ni metallic films have also been studied.[28,30] The XRD patterns of Ni films show similar results as the XRD patterns of NiO films discussed in the previous chapter. The peaks representing (110), (200) and (220) lattice planes of metallic Ni are observed. Therefore, we inferred that the crystal structure of Ni is face-centered cubic (fcc). We can calculate the theoretical growth rate of Ni as

$$\rho = \frac{4 \times M_{Ni}}{a^3 \times N_A}$$

where ρ represents the density of the compound (g/cm^3), a represents the cubic length (Å), N_A represents the Avogadro's number (mol^{-1}) and M represents the molar mass of the compound (g/mol). The unit cell length is then

$$a = \sqrt[3]{\frac{4 \times M_{Ni}}{\rho \times N_A}} = \sqrt[3]{\frac{4 \times 58.69}{8.908 \times 6.023 \times 10^{23}}} = 3.524 \text{ Å}$$

By giving the same assumption as NiO thin films. The estimated growth rate per cycle is calculated as

$$\text{gpc} = \frac{a}{\sqrt{3}} = 2.04\ \text{Å}$$

Table 3.1 lists the experiment growth rate of Ni metallic thin films under different conditions. We found that the estimated growth rate is higher than the experimental data. It is most likely due to the steric hindrance caused by large segments of adsorbed precursor, which will prevent any additional precursor to be adsorbed to the substrate. Precursor depletion and insufficient pulsing time may also cause the different between experimental data and calculated growth rate.

Table 3.1: The experimental growth rate of Ni metallic thin film using $Ni(dad)_2$ and tert-butylamine.

Ref.	Substrate	Cycles	Growth per cycle
Kerrigan et al.[28]	Pt substrate		0.60 Å
Kerrigan et al.[28]	Ru wafer	150~250	0.12 Å
Kerrigan et al.[28]	Ru wafer	>500	0.18 Å
Kerrigan et al.[28]	Ru wafer	>1000	0.44 Å

Chapter 4: Conclusions and Future Works

1. Conclusions

In Chapter 2, a reaction mechanism for NiO ALD was developed. In the proposed mechanism, the $NiCp_2$ precursor is adsorbed onto the substrate during the Ni precursor half cycle, then a Cp ligand is dissociated from the nickel precursor after the precursor is adsorbed onto the growth surface. During the subsequent O_3 half cycle, the Cp ligand that remained on the growth surface is then oxidized by ozone to produce CO_2 and H_2O. The theoretical growth rate of NiO films was calculated as 2.40 Å. In comparison to the experimental data, the difference may be caused by the steric hindrance effects, insufficient reactor purge, or precursor depletion. The calculated theoretical gpc is consistent with the experiment data deposited at ~250℃, which concludes that the deposition at ~250℃ is most likely to meet the theoretical conditions.

In Chapter 3, Ru ALD process and Ni metallic ALD processes were linked together as a novel method for generating a conformal nickel coating. We developed the reaction mechanism and calculated the growth per cycle. To find a growth rate for Ru as 2.19 Å/cycle and for Ni is 2.04 Å/cycle. It can be indicated that growth per cycle is relatively large comparing to the experimental data. The reason is probably also most likely due to the steric hindrance effect.

2. Future works

In this study, the reaction mechanism is developed based on the literature review and data analysis. The growth per cycle was calculated theoretically for different ideal ALD processes. One obvious addition is to extend these works to experiment, including studying the optimized deposition temperature and the exposure time for these ALD processes, confirming the reaction mechanism and analyzing the thin film properties by various techniques such as mass spectrometry, X-ray diffraction, and XPS. The experimental growth rate can also be obtained to compare with the theoretical growth rate to find out the condition which most likely to meet the ideal condition.

Bibliography

1. Ahvenniemi, E., Akbashev, A. R., Ali, S., Bechelany, M., Berdova, M., Boyadjiev, S., Cameron, D. C., Chen, R., Chubarov, M., Cremers, V., Devi, A., Drozd, V., Elnikova, L., Gottardi, G., Grigoras, K., Hausmann, D. M., Hwang, C. S., Jen, S.-H., Kallio, T., … Yurkevich, O. (2017). Review Article: Recommended reading list of early publications on atomic layer deposition—Outcome of the “Virtual Project on the History of ALD.” *Journal of Vacuum Science & Technology A: Vacuum, Surfaces, and Films*, *35*(1), 010801. https://doi.org/10.1116/1.4971389

2. Fryauf, D. M., Phillips, A. C., Bolte, M. J., Feldman, A., Tompa, G. S., & Kobayashi, N. P. (2018). Scaling Atomic Layer Deposition to Astronomical Optic Sizes: Low-Temperature Aluminum Oxide in a Meter-Sized Chamber [Research-article]. *ACS Applied Materials and Interfaces*, *10*(48), 41678–41689. https://doi.org/10.1021/acsami.8b10457

3. George, S. M. (2010). Atomic layer deposition: An overview. *Chemical Reviews*, *110*(1), 111–131. https://doi.org/10.1021/cr900056b

4. Levy, D. H., & Nelson, S. F. (2012). Thin-film electronics by atomic layer deposition. *Journal of Vacuum Science & Technology A: Vacuum, Surfaces, and*

Films, *30*(1), 018501. https://doi.org/10.1116/1.3670748

5. Puurunen, R. L. (2014). A short history of atomic layer deposition: Tuomo Suntola's atomic layer epitaxy. *Chemical Vapor Deposition*, *20*(10–12), 332–344. https://doi.org/10.1002/cvde.201402012
6. Salami, H., Poissant, A., & Adomaitis, R. A. (2017). Anomalously high alumina atomic layer deposition growth per cycle during trimethylaluminum under-dosing conditions. *Journal of Vacuum Science & Technology A: Vacuum, Surfaces, and Films*, *35*(1), 01B101. https://doi.org/10.1116/1.4963368
7. Salami, H., Uy, A., Vadapalli, A., Grob, C., Dwivedi, V., & Adomaitis, R. A. (2019). Atomic layer deposition of ultrathin indium oxide and indium tin oxide films using a trimethylindium, tetrakis(dimethylamino)tin, and ozone precursor system. *Journal of Vacuum Science & Technology A*, *37*(1), 010905. https://doi.org/10.1116/1.5058171
8. Mane, A. U., Allen, A. J., Kanjolia, R. K., & Elam, J. W. (2016). Indium Oxide Thin Films by Atomic Layer Deposition Using Trimethylindium and Ozone. *Journal of Physical Chemistry C*, *120*(18), 9874–9883. https://doi.org/10.1021/acs.jpcc.6b02657
9. Travis, C. D., & Adomaitis, R. A. (2013). Dynamic modeling for the design and cyclic operation of an atomic layer deposition (ALD) reactor. *Processes*, *1*(2),

128–152. https://doi.org/10.3390/pr1020128

10. Wank, J. R., George, S. M., & Weimer, A. W. (2004). Nanocoating individual cohesive boron nitride particles in a fluidized bed by ALD. *Powder Technology*, *142*(1), 59–69. https://doi.org/10.1016/j.powtec.2004.03.010

11. Biyikli, N., & Haider, A. (2017). Atomic layer deposition: An enabling technology for the growth of functional nanoscale semiconductors. *Semiconductor Science and Technology*, *32*(9), 93002. https://doi.org/10.1088/1361-6641/aa7ade

12. Johnson, R. W., Hultqvist, A., & Bent, S. F. (2014). A brief review of atomic layer deposition: From fundamentals to applications. *Materials Today*, *17*(5), 236–246. https://doi.org/10.1016/j.mattod.2014.04.026

13. Black, J. K., Brunton, A. N., Bannister, N. P., Deines-Jones, P., & Jahoda, K. (2003). The imaging X-ray detector for Lobster-ISS. *Nuclear Instruments and Methods in Physics Research, Section A: Accelerators, Spectrometers, Detectors and Associated Equipment*, *513*(1-2 SPEC. ISS.), 123–126. https://doi.org/10.1016/j.nima.2003.08.015

14. Utriainen, M., Kröger-Laukkanen, M., Johansson, L. S., & Niinistö, L. (2000). Studies of metallic thin film growth in an atomic layer epitaxy reactor using M(acac)2 (M = Ni, Cu, Pt) precursors. *Applied Surface Science*, *157*(3), 151–158. https://doi.org/10.1016/S0169-4332(99)00562-0

15. Lu, H. L., Scarel, G., Wiemer, C., Perego, M., Spiga, S., Fanciulli, M., & Pavia, G. (2008). Atomic Layer Deposition of NiO Films on Si(100) Using Cyclopentadienyl-Type Compounds and Ozone as Precursors. *Journal of The Electrochemical Society*, *155*(10), H807. https://doi.org/10.1149/1.2965456

16. Bachmann, J., Zolotaryov, A., Albrecht, O., Goetze, S., Berger, A., Hesse, D., Novikov, D., & Nielsch, K. (2011). Stoichiometry of nickel oxide films prepared by ALD. *Chemical Vapor Deposition*, *17*(7–9), 177–180. https://doi.org/10.1002/cvde.201004300

17. Wen, Y., Cai, J., Zhang, J., Yang, J., Shi, L., Cao, K., Chen, R., & Shan, B. (2019). Edge-Selective Growth of MCp2 (M = Fe, Co, and Ni) Precursors on Pt Nanoparticles in Atomic Layer Deposition: A Combined Theoretical and Experimental Study. *Chemistry of Materials*, *31*(1), 101–111. https://doi.org/10.1021/acs.chemmater.8b03168

18. Yu, L., Wang, G., Wan, G., Wang, G., Lin, S., Li, X., Wang, K., Bai, Z., & Xiang, Y. (2016). Highly effective synthesis of NiO/CNT nanohybrids by atomic layer deposition for high-rate and long-life supercapacitors. *Dalton Transactions*, *45*(35), 13779–13786. https://doi.org/10.1039/c6dt01927g

19. Zhang, J., Chen, C., Yan, W., Duan, F., Zhang, B., Gao, Z., & Qin, Y. (2016). Ni nanoparticles supported on CNTs with excellent activity produced by atomic

layer deposition for hydrogen generation from the hydrolysis of ammonia borane. *Catalysis Science and Technology*, *6*(7), 2112–2119. https://doi.org/10.1039/c5cy01497b

20. Aaltonen, T., Petra Alen, Ritala, M., & Leskelä, M. (2003). Ruthenium Thin Films Grown by Atomic Layer Deposition. *Chemical Vapor Deposition*, 45–49. https://doi.org/10.1126/science.1194140

21. Aaltonen, T., Ritala, M., Arstila, K., Keinonen, J., & Leskelä, M. (2004). Atomic layer deposition of ruthenium thin films from Ru(thd)3 and oxygen. *Chemical Vapor Deposition*, *10*(4), 215–219. https://doi.org/10.1002/cvde.200306288

22. Hong, T. E., Choi, S.-H., Yeo, S., Park, J.-Y., Kim, S.-H., Cheon, T., Kim, H., Kim, M.-K., & Kim, H. (2013). Atomic Layer Deposition of Ru Thin Films Using a Ru(0) Metallorganic Precursor and O 2 . *ECS Journal of Solid State Science and Technology*, *2*(3), P47–P53. https://doi.org/10.1149/2.001303jss

23. Gao, Z., Le, D., Khaniya, A., Dezelah, C. L., Woodruff, J., Kanjolia, R. K., Kaden, W. E., Rahman, T. S., & Banerjee, P. (2019). Self-Catalyzed, Low-Temperature Atomic Layer Deposition of Ruthenium Metal Using Zero-Valent Ru(DMBD)(CO) 3 and Water. *Chemistry of Materials*, *31*(4), 1304–1317. https://doi.org/10.1021/acs.chemmater.8b04456

24. Eom, T. K., Sari, W., Choi, K. J., Shin, W. C., Kim, J. H., Lee, D. J., Kim, K. B.,

Sohn, H., & Kim, S. H. (2009). Low temperature atomic layer deposition of ruthenium thin films using isopropylmethylbenzene-cyclohexadiene-ruthenium and O2. *Electrochemical and Solid-State Letters*, *12*(11), 85–88. https://doi.org/10.1149/1.3207867

25. Yeo, S., Choi, S. H., Park, J. Y., Kim, S. H., Cheon, T., Lim, B. Y., & Kim, S. (2013). Atomic layer deposition of ruthenium (Ru) thin films using ethylbenzen-cyclohexadiene Ru(0) as a seed layer for copper metallization. *Thin Solid Films*, *546*, 2–8. https://doi.org/10.1016/j.tsf.2013.03.074
26. Lim, B. S., Rahtu, A., & Gordon, R. G. (2003). Atomic layer deposition of transition metals. *Nature Materials*, *2*(11), 749–754. https://doi.org/10.1038/nmat1000
27. Kalutarage, L. C., Martin, P. D., Heeg, M. J., & Winter, C. H. (2013). Volatile and thermally stable mid to late transition metal complexes containing α-imino alkoxide ligands, a new strongly reducing coreagent, and thermal atomic layer deposition of Ni, Co, Fe, and Cr metal films. *Journal of the American Chemical Society*, *135*(34), 12588–12591. https://doi.org/10.1021/ja407014w
28. Kerrigan, M. M., Klesko, J. P., Blakeney, K. J., & Winter, C. H. (2018). Low Temperature, Selective Atomic Layer Deposition of Nickel Metal Thin Films. *ACS Applied Materials and Interfaces*, *10*(16), 14200–14208.

https://doi.org/10.1021/acsami.8b03074

29. Wolf, S., Breeden, M., Ueda, S., Woodruff, J., Moinpour, M., Kanjolia, R., & Kummel, A. (2020). The role of oxide formation on insulating versus metallic substrates during Co and Ru selective ALD. *Applied Surface Science*, *510*(November 2019). https://doi.org/10.1016/j.apsusc.2019.144804

30. Holden, K. E. K., Dezelah, C. L., & Conley, J. F. (2019). Atomic Layer Deposition of Transparent p-Type Semiconducting Nickel Oxide Using Ni(tBu2DAD)2 and Ozone [Research-article]. *ACS Applied Materials and Interfaces*, *11*(33), 30437–30445. https://doi.org/10.1021/acsami.9b08926

31. Kerrigan, M. M., Klesko, J. P., & Winter, C. H. (2017). Low Temperature, Selective Atomic Layer Deposition of Cobalt Metal Films Using Bis(1,4-di-tert-butyl-1,3-diazadienyl)cobalt and Alkylamine Precursors. *Chemistry of Materials*, *29*(17), 7458–7466. https://doi.org/10.1021/acs.chemmater.7b02456